Supporting materials

Nitrate-induced and in-situ electrochemical activation synthesis of oxygen deficiencies-rich nickel/nickel (oxy)hydroxide hybrid films for enhanced electrocatalytic water splitting

M. Y. Gao[a], C. B. Sun[a], H. Lei[a], J.R. Zeng[a] and Q.B. Zhang[a,b*]

[a] Key Laboratory of Ionic Liquids Metallurgy, Faculty of Metallurgical and Energy Engineering, Kunming University of Science and Technology, Kunming, 650093, P.R. China

[b] State Key Laboratory of Complex Nonferrous Metal Resources Cleaning Utilization in Yunnan Province, Kunming 650093, P.R. China

*Corresponding author. Tel: +86-871-65162008; Fax: +86-871-65161278.

E-mail address: qibozhang@kmust.edu.cn (Q.B. Zhang)

Experimental section

Chemicals: choline chloride (ChCl), ethylene glycol (EG), nickel nitrate hexahydrate ($Ni(NO_3)_2 \cdot 6H_2O$), nickel chloride hexahydrate ($NiCl_2 \cdot 6H_2O$), potassium hydroxide (KOH), hydrochloric acid (HCl) and ethyl alcohol (C_2H_5OH) were purchased from Aladdin Ltd. (Shanghai China). All the chemicals were analytical grade and used as received without further purification.

Synthesis of nickel/nickel hydroxide hybrid films: The nickel/nickel hydroxide hybrid films directly grown on Cu foil were prepared via a facile one-step electrodeposition process performed in the Ethaline, a typical deep eutectic solvent (DES) with a molar ratio of ChCl/EG (1:2). To optimize the deposit, the total mole of nickel in the electrolyte were maintained at 0.50 M while the molar ratio of Ni^{2+} and NO_3^- systematically varied, such as, 0.50 M $NiCl_2 \cdot 6H_2O$, 0.45 M $NiCl_2 \cdot 6H_2O$ + 0.05 M $Ni(NO_3)_2 \cdot 6H_2O$ (ratio of 9:1), 0.25 M $NiCl_2 \cdot 6H_2O$ + 0.25 M $Ni(NO_3)_2 \cdot 6H_2O$ (ratio of 1:1), 0.50 M $Ni(NO_3)_2 \cdot 6H_2O$, etc. The deposition process was conducted in a typical three-electrode cell at 343 K with a Cu foil, two parallel-arranged graphite flakes, and an Ag/Ag^+ (0.01 M AgCl/Ethaline) electrode as the working electrode, counter electrode and reference electrode, respectively. The deposition potential was carried out at -0.85 V vs. Ag/Ag^+ based on the cyclic voltammogram (CV) investigations as shown in Figure S1, with an optimized charge density of 5 C cm^{-2}. Prior to electrodeposition, the Cu foil (0.47 cm^2) was rinsed in ethanol for 5 min, then ultrasonically cleaned in 1vol.% HCl for 5 min, subsequently washed with deionized water, and finally dried in room temperature. After deposition, the obtained samples were cleaned by ethanol and deionized water for repeated several times.

Materials Characterization: The crystal structure of the deposited samples was recorded using an X-ray diffraction pattern (XRD, Bruker D8 Advanced Diffractometer with Cu Kα radiation). The microstructure and elemental composition of the prepared samples were determined by field emission scanning electron microscope (FE-SEM, NOVA NanoSEM 450) and transmission electron microscope (TEM, Tecnai G2 F30) with equipping an energy-dispersive X-ray (EDX) system. Additionally, the surface chemical states of the samples were analyzed via X-ray photoelectron spectroscopy (XPS, PHI 550). Raman spectra were conducted on a Renishaw Raman microscope using 514 nm laser excitation at room temperature with a laser power of 5 mW. Photoluminescence (PL) spectra was investigated using an FLs980 full-function steady/transient fluorescence spectrometer (Edinburgh, UK) with a Xe lamp as the excitation light source at room temperature. UV-vis spectra were obtained with Hitachi spectrometer U-3900H using 1 cm quartz cuvettes. The conductivity and viscosity of the electrolyte systems with various molar ratio of Ni^{2+} and NO_3^- were measured using a DDS-12DW benchtop conductivity meter (BANTE Instruments, Shanghai, China) at room temperature and a rotary viscometer (SNB-2, Shanghai Nirun Intelligent Technology, China), respectively.

Electrochemical characterization: All electrochemical measurements were conducted in 1.0 M KOH solution at 298 K by a CHI 760E electrochemical workstation in a three-electrode system with the as-deposited samples as the working electrode, a graphite rod counter electrode and Hg/HgO reference electrode. The Hg/HgO electrode was calibrated with the reversible hydrogen electrode (RHE), whose value was calculated to be (0.096 + 0.0591pH)

V vs. RHE. The electrocatalytic activities of HER and OER were measured by linear sweep voltammetry (LSV) curves at a scan rate of 5 mV s^{-1} with high-purity N_2 saturation. Electrochemical impedance spectroscopy (EIS) was recorded at a certain overpotential over a frequency range from 5 mHz to 1000 kHz with a 5 mV amplitude AC signal. The stability test was performed at 10 mA cm^{-2} for 24 h long-term electrolysis towards HER/OER, or by repeatedly switching between HER and OER at 10 mA cm^{-2}. The electrochemical double layer capacitance was evaluated to measure the electrochemical surface active area of the catalysts by using CV curves with potential range from 0.1 V to 0.2 V vs. RHE at different scan rates ranging from 20 to 200 mV s^{-1}. All data of the above experiments were present without *iR* compensation.

Calculation of the turnover frequency (TOF): The TOF values were evaluated based on CV measurements in 2.0 M phosphate buffer aqueous solution (PBS, pH=7.0) with potential ranging from -0.2 V ~ +0.6 V vs. RHE at a scan rate of 50 mV s^{-1}. Assuming one electron redox process, the integrated charge over the whole potential range was divided by two. Then, the value was divided by the Faraday constant to get the number of active sites for different samples, which can be obtained according to equation (1), and the turnover frequency (s^{-1}) can be calculated according to equation (2):[1]

$$n = \frac{Q}{2F} \quad (1)$$

$$TOF = \frac{I}{2nF} \quad (2)$$

where Q is the absolute charge recorded during a single CV measurement in 2.0 M PBS, F is the Faraday constant, and I is the current obtained during a LSV measurement in 1.0 M KOH.

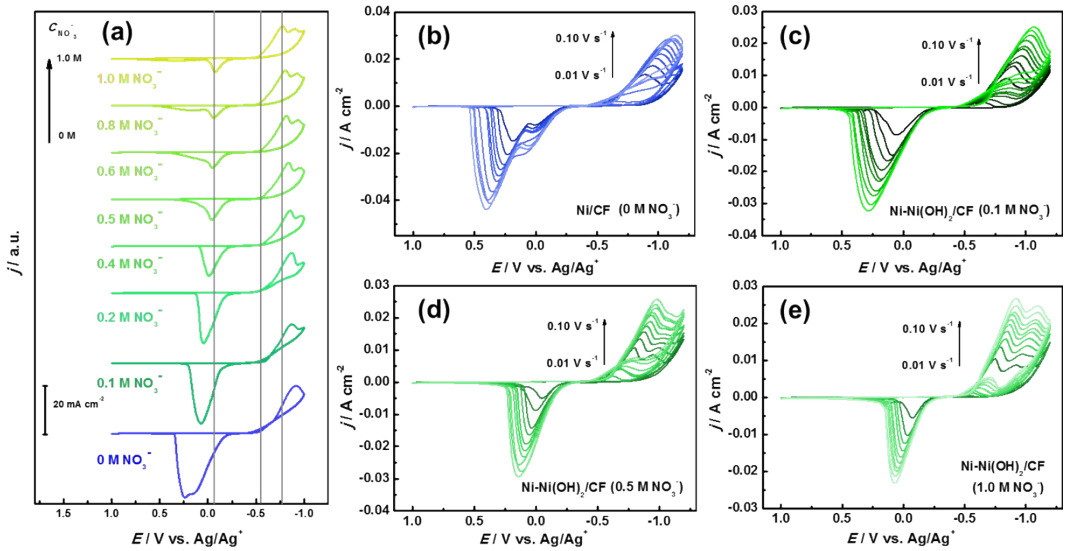

Figure S1. (a) CVs of Ethaline with different addition ratios of Ni^{2+}:NO_3^- (the total nickel mole was maintained at 0.50 M) recorded on a Pt disk electrode at 343 K at a scan rate of 20 mV s^{-1}. (b-e) The corresponding CVs for the reduction of Ni(II) species in Ethaline with different concentrations of NO_3^- recorded at various scan rates (indicated). It is obvious that upon the adding of nitrate ions, the cathodic reduction peak for Ni(II) is found to positively shift with the associated anodic peak occurred negatively shifting, which leads to a decrease in the potential difference between the cathodic peak and the anodic peak, revealing that the presence of nitrate ions plays a promoted effect (facilitating the charge transfer, Table S1) on the electrochemical reduction kinetics for the Ni(II) species with increasing the irreversible feature. In addition, the added cathodic peaks obtained at a higher concentration of NO_3^- suggesting the reduction of nitrate ions.

Table S1 Data of CV investigations with various scan rates

	Ni/CF (0 M NO_3^-)	Ni-$Ni(OH)_2$/CF (0.1 M NO_3^-)	Ni-$Ni(OH)_2$/CF (0.5 M NO_3^-)	Ni-$Ni(OH)_2$/CF (1.0 M NO_3^-)
α	0.0987	0.1266	0.1678	0.1718
$D_0*10^{-7}/cm^2\ s^{-1}$	8.273	4.23	3.613	3.66

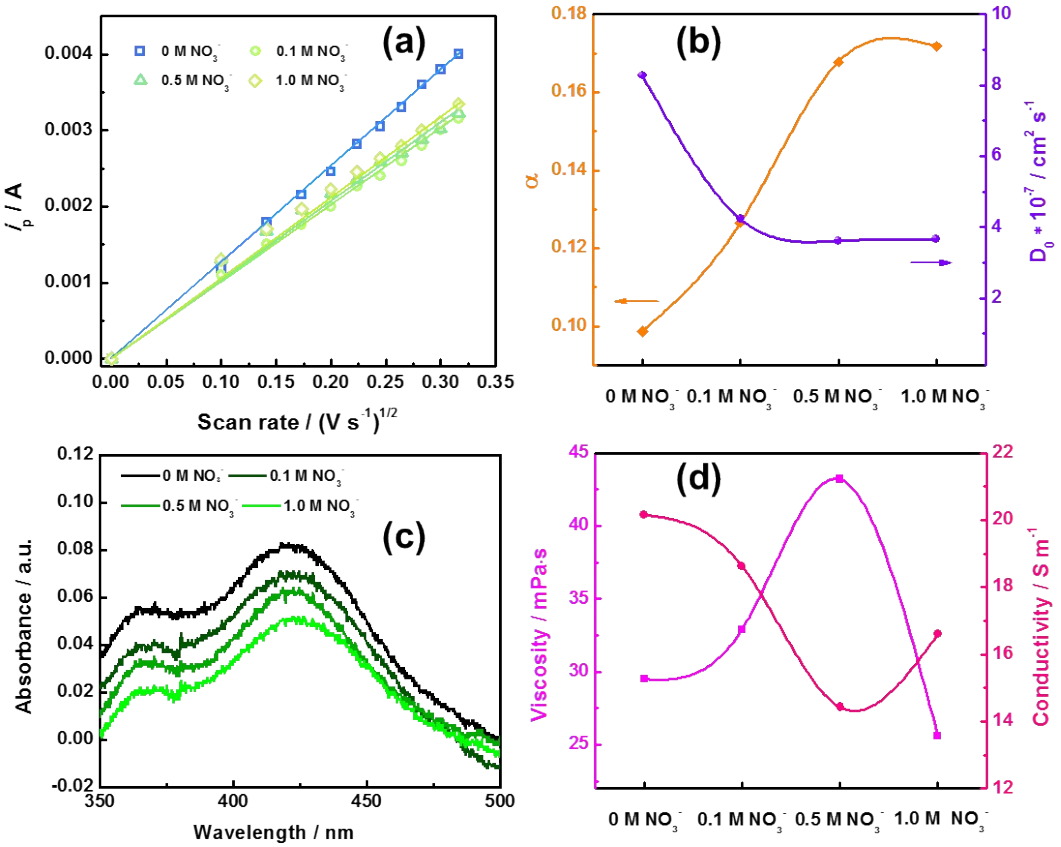

Figure S2. (a) The linear correlations of the cathodic peak current against the square root of sweep rate at various electrolyte systems with different concentrations of nitrate ions (indicated). The influence of nitrate ions on (b) charge transfer and diffusion coefficient of Ni(II) species, (c) UV-Vis spectra, and (d) conductivity and viscosity of the electrolyte systems. The presence of NO_3^- has little influence on the Ni(II) species in the electrolyte system, but has great influence on the conductivity and viscosity, which leads to changes on the charge transfer and diffusion coefficient of the Ni(II) species.

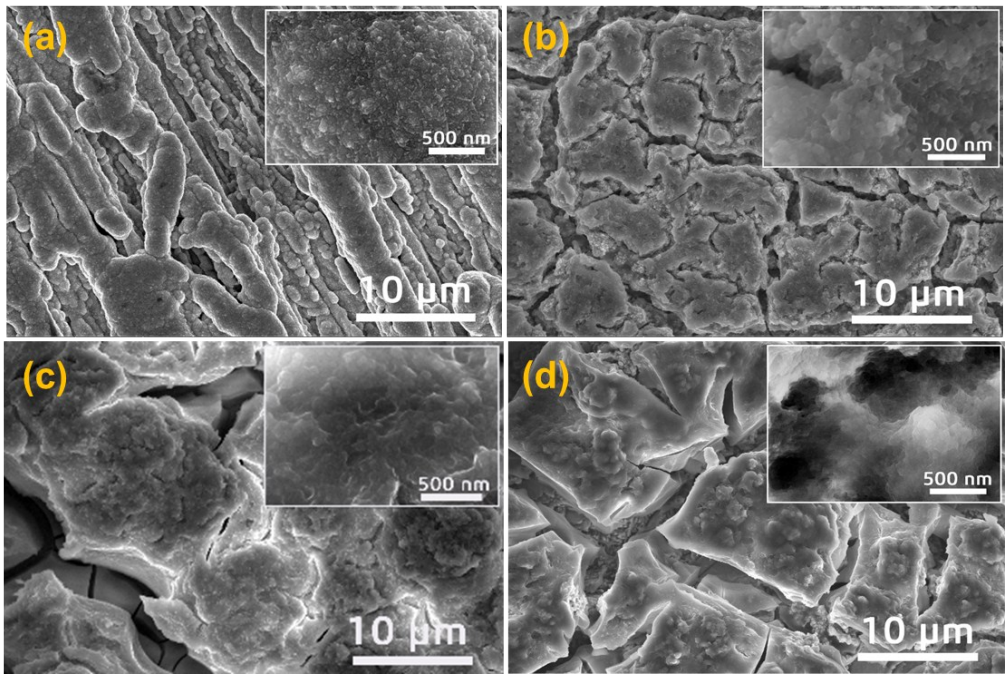

Figure S3. SEM images of the as-deposited Ni samples obtained from Ethaline with various addition concentrations of nitrate ions. (a) Ni/CF (0 M NO_3^-), (b) Ni-Ni(OH)$_2$/CF (0.1 M NO_3^-), (c) Ni-Ni(OH)$_2$/CF (0.5 M NO_3^-), (d) Ni-Ni(OH)$_2$/CF (1.0 M NO_3^-). The Ni/CF exhibits an irregular structure (Figure S3a), while the introduction of nitrate ions results in a nanoparticles assembled surface filled with crevices (Figure S3b). The surface crevices develops more severe with further increase the concentrations of nitrate ions to 0.5 and 1.0 M (Figure S3c,d), which results in non-compact and loose structure, and thus goes against the catalytic performance.

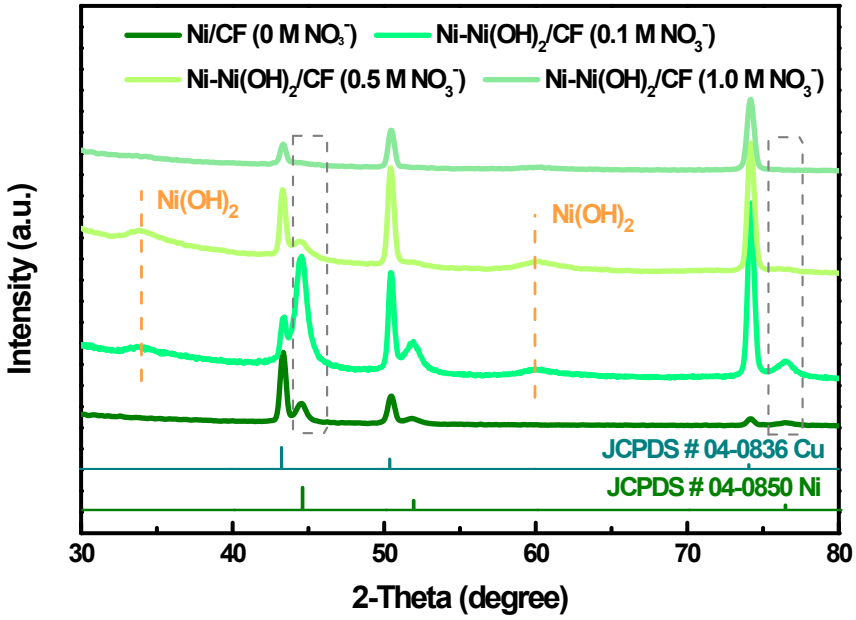

Figure S4. XRD patterns of the as-deposited Ni samples obtained from Ethaline with various addition concentrations of nitrate ions. (a) 0 M NO_3^-, (b) 0.1 M NO_3^-, (c) 0.5 M NO_3^-, (d) 1.0 M NO_3^-.

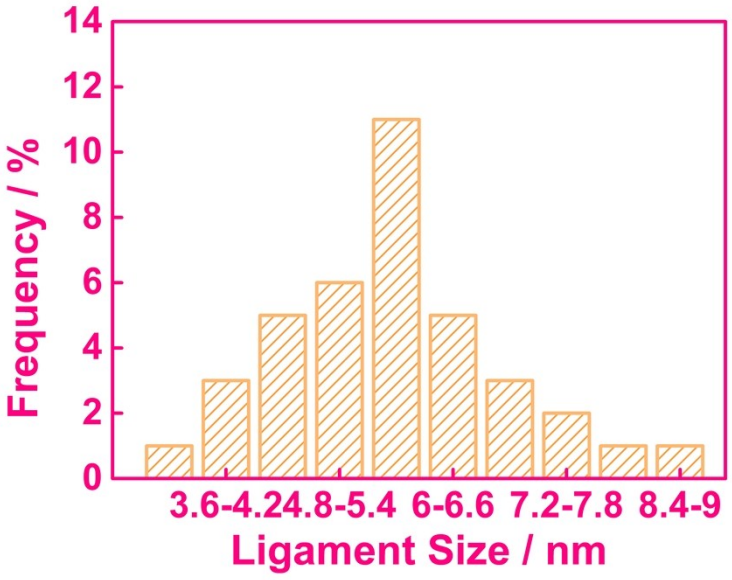

Figure S5. The particle size distribution of the as-prepared Ni-Ni(OH)$_2$/CF.

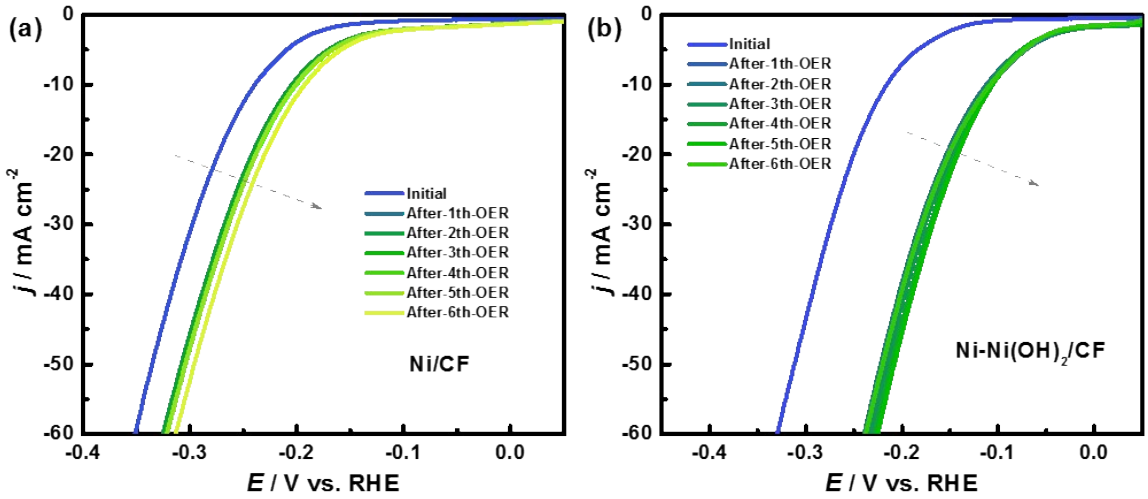

Figure S6. Polarization curves recorded with (a) Ni/CF and (b) Ni-Ni(OH)$_2$/CF during 6 rounds of continuous potential scanning in the OER region (from 1.2 to 1.9 V vs. RHE). In both cases, significant enhancement on the HER activity of the deposited materials upon in-situ OER activation is observed and the catalytic performance becomes stable after 6 rounds of scanning.

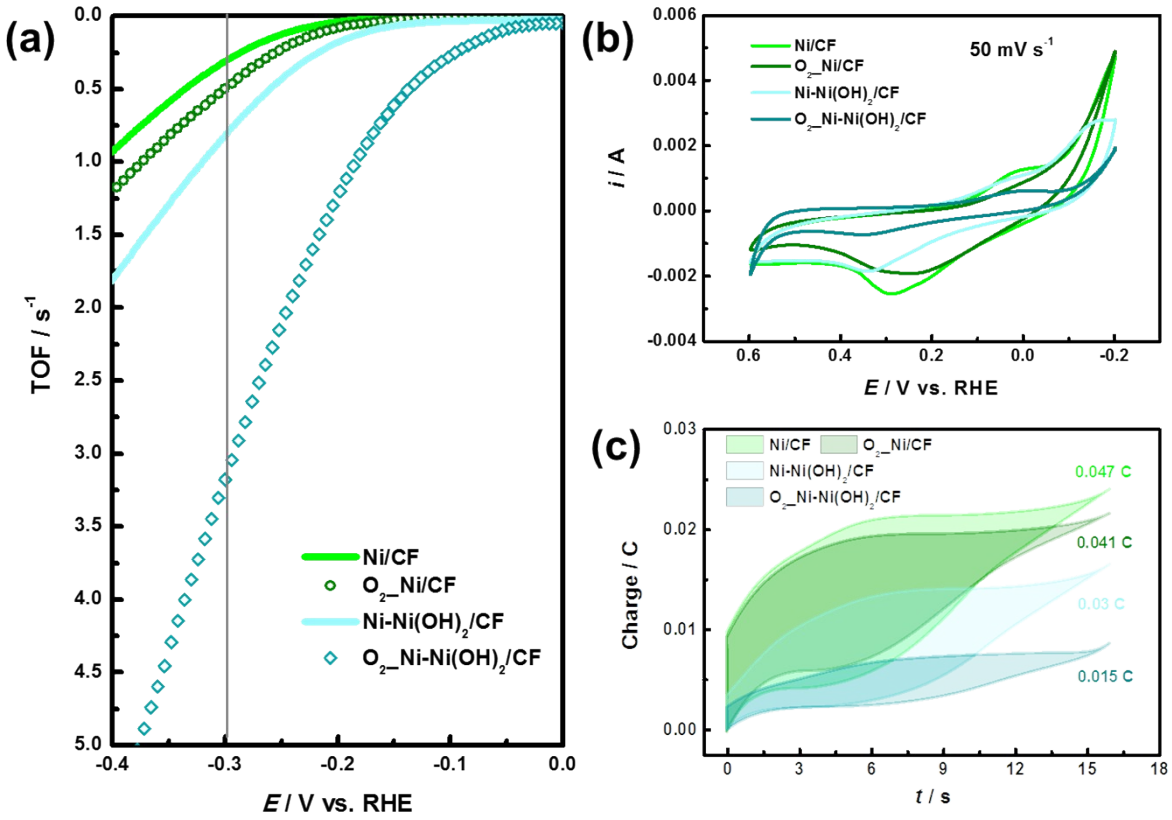

Figure S7. (a) The calculated TOF curves of Ni/CF, Ni-Ni(OH)$_2$/CF, O_2_Ni/CF, and O_2_Ni-Ni(OH)$_2$/CF. (b, c) The corresponding CVs and calculated charge in 2.0 M PBS at a scan rate of 50 mV s^{-1}.

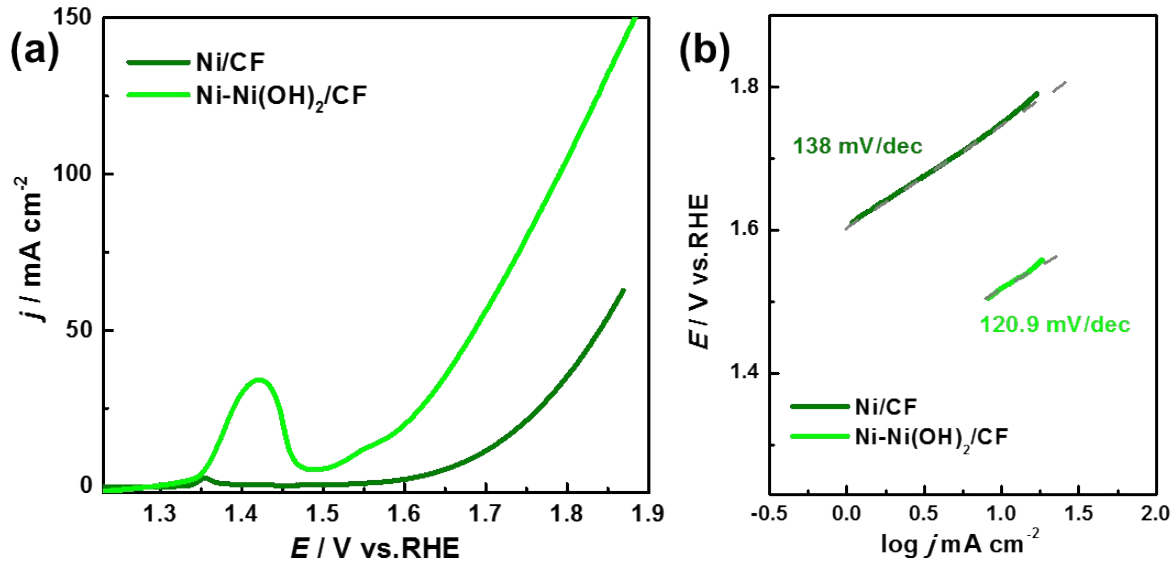

Figure S8. (a) Polarization curves of Ni/CF and Ni-Ni(OH)$_2$ towards OER. (b) The associated Tafel plots.

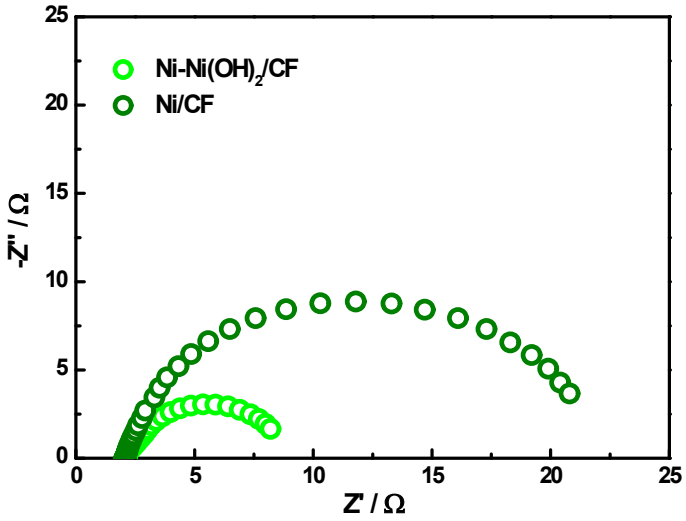

Figure S9. Nyquist plots of Ni/CF and Ni-Ni(OH)$_2$ at an overpotential of 350 mV.

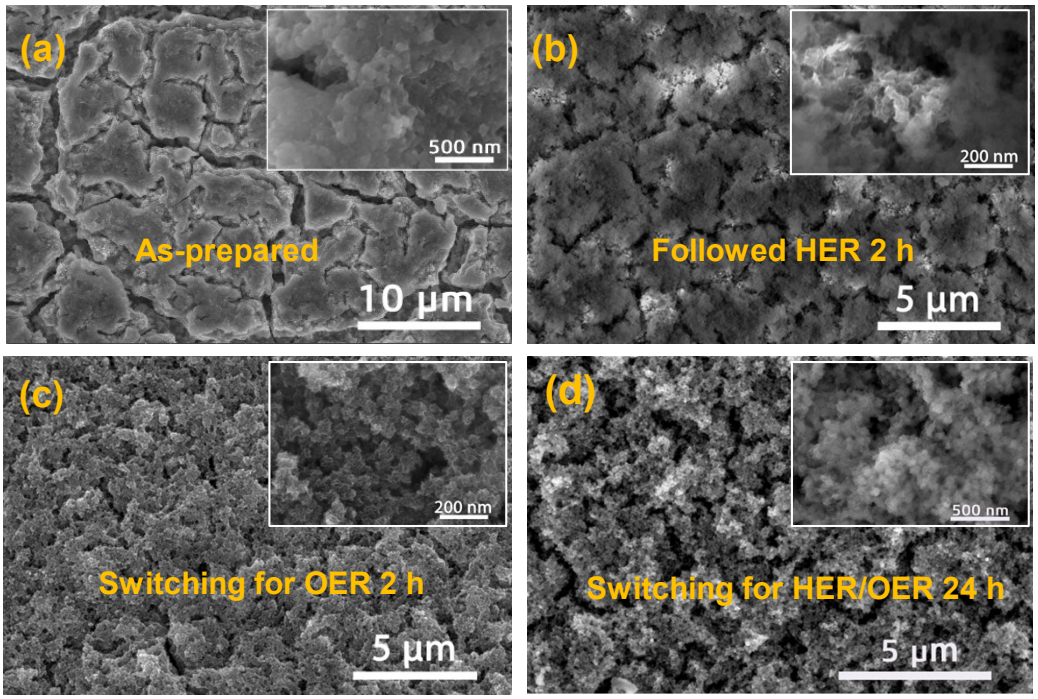

Figure S10. SEM images for Ni-Ni(OH)$_2$/CF after switching operation (HER and OER in turn) for 24 h, which shows the switchable stability of the O_2_Ni-Ni(OH)$_2$/CF. The highly porous structure of the O_2_Ni-Ni(OH)$_2$/CF can be well retained.

Table S2 Comparison of the HER performance with previously reported Ni-based HER catalyst in a basic solution

Catalysts	Electrolyte	Overpotential / mV @10 mA cm^{-2}	Tafel slope / mV dec^{-1}	Ref.
Ni-$Ni(OH)_2$/CF	1 M KOH	η_{10} = 110	83.9	This work
CP@Ni-P	1 M KOH	η_{10} = 117	85.4	2
Ni/MWCNT	1 M KOH	η_{10} = ~350	102	3
$Ni_2P/Ni_{12}P_5$	1 M KOH	η_{10} = 234	98	4
Ni_xP/CNT	1 M KOH	η_{10} = 109	119.8	5
NiFe composite/microporous	1 M KOH	η_{10} = 219	116	6
Ni_3S_2 /nanoparticles	1 M KOH	η_{10} = 480	102	7
Ni_3S_2 /nanosheets	1 M KOH	η_{10} = 170	– –	8
NiCoZn /porous	1 M KOH	– –	96	9
$NiCo_2S_4$ /nanowires	1 M KOH	– –	141	10
NiFe/nanoparticles	1 M KOH	η_{10} = 219	111	11
MnNi	0.1 M KOH	η_{10} = ~360	– –	12
Ni_xP_y-325	1 M KOH	– –	107.3	13
NiFe LDH/NF	1 M KOH	η_{10} = 210	– –	14
NiFeP/NiFe	1 M KOH	η_{10} = 255	– –	15
NiS_2NA/CC	1 M KOH	η_{10} = 149	104	16
Ni_3S_2/NF	1 M KOH	η_{10} = 123	118	17

Table S3 Comparison of the OER performance with previously reported Ni-based OER catalysts in a basic solution

Catalysts	Electrolyte	Overpotential/ mV @10 mA cm^{-2}	Ref.
Ni-$Ni(OH)_2$/CF	1 M KOH	η_{10} = 290	This work
NiO_x	1 M KOH	η_1 = 300	18
NiO_x	1 M NaOH	H_{10} = ~440	19
NiO nanoplates	1 M KOH	η_{10} = 430	20
$Ni(OH)_2$ nanoplates	1 M KOH	η_{10} = 360	20
$Ni(OH)_2$ nanoparticles	1 M KOH	η_{10} = 299	21
NiO_x nanoparticles	1 M KOH	η_{10} = 331	21
porous NiO/NF	1 M KOH	η_{10} = 310	22

NiO_x/Ni	1 M KOH	η_{10} = 390	23
NiO/TiO_2	1 M KOH	η_{10} = 390	24
Ni/NiO(OH)/NC	0.1 M KOH	η_{10} = 390	25
α-$Ni(OH)_2$	0.1 M KOH	η_{10} = 331	26
$Ni(OH)_2$/NF	1 M KOH	η_{10} = 350	27
β-$Ni(OH)_2$	1 M KOH	η_{10} = 340	28
Porous β-$Ni(OH)_2$ nanosheets	1 M KOH	η_{10} = 415	29
$Ni(OH)_2$/Ni	1 M NaOH	η_{10} = ~340	30
Ni_2P nanoparticle	1 M KOH	η_{10} = 290	31
$Ni_{12}P_5$/NF	1 M KOH	η_{10} = 295	32
$NiCo_2O_4$ nanosheets	1 M KOH	η_{10} = 320	33
Ni-doped Co_3O_4 porous	1 M KOH	η_{10} = 530	34
Core-shell Ni-Co Nanowire	1 M KOH	η_{10} = 302	35
NiCo LDH nanosheets	1 M KOH	η_{10} = 367	36
$NiCo_2O_4$ nanowires	1 M KOH	η_{10} = 360	37
$Ni_xCo_{3-x}O_4$ nanowires	1 M KOH	η_{10} = 370	38
$NiCo_2O_4$ nanocages	1 M KOH	η_{10} = 380	39
Ni/Mo_2C-porpos carbon supported	1 M KOH	η_{10} = 368	40
Single-layer NiFe-LDH	1 M KOH	η_{10} = ~300	41
G-Ni_4Fe/GF	1 M KOH	η_{10} = 310	42
Ni_3FeN nanoparticles	1 M KOH	η_{10} = 280	43
nNiFe LDH/NGF	1 M KOH	η_{10} = 337	44

Reference

1. D. Merki, S. Fierro, H. Vrubel and X. Hu, *Chemical Science*, 2011, **2**, 1262-1267.
2. X. Wang, W. Li, D. Xiong, D. Y. Petrovykh and L. Liu, *Advanced Functional Materials*, 2016, **26**, 4067-4077.
3. M. A. McArthur, L. Jorge, S. Coulombe and S. Omanovic, *Journal of Power Sources*, 2014, **266**, 365-373.
4. S. Surendran, S. Shanmugapriya, S. Shanmugam, L. Vasylechko and R. Kalai Selvan, *ACS Applied Energy Materials*, 2018, **1**, 78-92.
5. S. Wang, L. Zhang, X. Li, C. Li, R. Zhang, Y. Zhang and H. Zhu, *Nano Research*, 2016, **10**, 415-425.
6. R. Solmaz and G. Kardaş, *Electrochimica Acta*, 2009, **54**, 3726-3734.
7. T.-W. Lin, C.-J. Liu and C.-S. Dai, *Applied Catalysis B: Environmental*, 2014, **154-155**, 213-220.
8. L. L. Feng, G. Yu, Y. Wu, G. D. Li, H. Li, Y. Sun, T. Asefa, W. Chen and X. Zou, *Journal of the American Chemical Society*, 2015, **137**, 14023-14026.

9. R. Solmaz, A. Döner, İ. Şahin, A. O. Yüce, G. Kardaş, B. Yazıcı and M. Erbil, *International Journal of Hydrogen Energy*, 2009, **34**, 7910-7918.
10. D. Liu, Q. Lu, Y. Luo, X. Sun and A. M. Asiri, *Nanoscale*, 2015, **7**, 15122-15126.
11. X. Zhang, H. Xu, X. Li, Y. Li, T. Yang and Y. Liang, *ACS Catalysis*, 2015, **6**, 580-588.
12. M. Ledendecker, G. Clavel, M. Antonietti and M. Shalom, *Advanced Functional Materials*, 2015, **25**, 393-399.
13. J. Li, J. Li, X. Zhou, Z. Xia, W. Gao, Y. Ma and Y. Qu, *ACS applied materials & interfaces*, 2016, **8**, 10826-10834.
14. J. S. Luo, J. H. Im, M. T. Mayer, M. Schreier, M. K. Nazeeruddin, N. G. Park, S. D. Tilley, H. J. Fan and M. Gratzel, *Science*, 2014, **345**, 1593-1596.
15. C. G. Read, J. F. Callejas, C. F. Holder and R. E. Schaak, *ACS applied materials & interfaces*, 2016, **8**, 12798-12803.
16. C. Tang, Z. Pu, Q. Liu, A. M. Asiri and X. Sun, *Electrochimica Acta*, 2015, **153**, 508-514.
17. C. Tang, Z. Pu, Q. Liu, A. M. Asiri, Y. Luo and X. Sun, *International Journal of Hydrogen Energy*, 2015, **40**, 4727-4732.
18. L. Trotochaud, J. K. Ranney, K. N. Williams and S. W. Boettcher, *Journal of the American Chemical Society*, 2012, **134**, 17253-17261.
19. C. C. McCrory, S. Jung, J. C. Peters and T. F. Jaramillo, *Journal of the American Chemical Society*, 2013, **135**, 16977-16987.
20. X.-Y. Yu, Y. Feng, B. Guan, X. W. Lou and U. Paik, *Energy & Environmental Science*, 2016, **9**, 1246-1250.
21. L. A. Stern and X. Hu, *Faraday discussions*, 2014, **176**, 363-379.
22. P. T. Babar, A. C. Lokhande, M. G. Gang, B. S. Pawar, S. M. Pawar and J. H. Kim, *Journal of Industrial and Engineering Chemistry*, 2018, **60**, 493-497.
23. G.-Q. Han, Y.-R. Liu, W.-H. Hu, B. Dong, X. Li, X. Shang, Y.-M. Chai, Y.-Q. Liu and C.-G. Liu, *Applied Surface Science*, 2015, **359**, 172-176.
24. Y. Zhao, X. Jia, G. Chen, L. Shang, G. I. Waterhouse, L. Z. Wu, C. H. Tung, D. O'Hare and T. Zhang, *Journal of the American Chemical Society*, 2016, **138**, 6517-6524.
25. J. Ren, M. Antonietti and T.-P. Fellinger, *Advanced Energy Materials*, 2015, **5**, 1401660.
26. M. Gao, W. Sheng, Z. Zhuang, Q. Fang, S. Gu, J. Jiang and Y. Yan, *Journal of the American Chemical Society*, 2014, **136**, 7077-7084.
27. J. Lee, G.-H. Lim and B. Lim, *Chemical Physics Letters*, 2016, **644**, 51-55.
28. S. C. Jung, S. L. Sim, Y. W. Soon, C. M. Lim, P. Hing and J. R. Jennings, *Nanotechnology*, 2016, **27**, 275401.
29. H. F. Liang, L. S. Li, F. Meng, L. N. Dang, J. Q. Zhuo, A. Forticaux, Z. C. Wang and S. Jin, *Chem Mater*, 2015, **27**, 5702-5711.
30. J. S. Luo, J. H. Im, M. T. Mayer, M. Schreier, M. K. Nazeeruddin, N. G. Park, S. D. Tilley, H. J. Fan and M. Gratzel, *Science*, 2014, **345**, 1593-1596.
31. L.-A. Stern, L. Feng, F. Song and X. Hu, *Energy & Environmental Science*, 2015, **8**, 2347-2351.
32. P. W. Menezes, A. Indra, C. Das, C. Walter, C. Göbel, V. Gutkin, D. Schmeiβer and M. Driess, *ACS Catalysis*, 2016, **7**, 103-109.
33. J. Bao, X. Zhang, B. Fan, J. Zhang, M. Zhou, W. Yang, X. Hu, H. Wang, B. Pan and Y. Xie, *Angewandte Chemie*, 2015, **54**, 7399-7404.
34. X. Zou, J. Su, R. Silva, A. Goswami, B. R. Sathe and T. Asefa, *Chem Commun (Camb)*, 2013, **49**, 7522-7524.
35. S.-H. Bae, J.-E. Kim, H. Randriamahazaka, S.-Y. Moon, J.-Y. Park and I.-K. Oh, *Advanced Energy Materials*, 2017, **7**, 1601492.
36. H. Liang, F. Meng, M. Caban-Acevedo, L. Li, A. Forticaux, L. Xiu, Z. Wang and S. Jin, *Nano letters*, 2015, **15**, 1421-1427.
37. Z. Peng, D. Jia, A. M. Al-Enizi, A. A. Elzatahry and G. Zheng, *Advanced Energy Materials*, 2015, **5**, 1402031.
38. Y. Li, P. Hasin and Y. Wu, *Advanced materials*, 2010, **22**, 1926-1929.
39. L. Han, X. Y. Yu and X. W. Lou, *Advanced materials*, 2016, **28**, 4601-4605.
40. Z. Y. Yu, Y. Duan, M. R. Gao, C. C. Lang, Y. R. Zheng and S. H. Yu, *Chem Sci*, 2017, **8**, 968-973.
41. F. Song and X. Hu, *Nature Communications,* 2014, **5**, 4477.
42. X. Yu, M. Zhang, Y. Tong, C. Li and G. Shi, *Advanced Energy Materials*, 2018, **8**, 1800403.
43. X. Jia, Y. Zhao, G. Chen, L. Shang, R. Shi, X. Kang, G. I. N. Waterhouse, L.-Z. Wu, C.-H. Tung and T. Zhang, *Advanced Energy Materials*, 2016, **6**, 1502585.
44. C. Tang, H. S. Wang, H. F. Wang, Q. Zhang, G. L. Tian, J. Q. Nie and F. Wei, *Advanced materials*, 2015, **27**, 4516-4522.